Heat Transfer

WILEY

HEAT TRANSFER

ORIGINAL ARTICLE

Thermodynamic Irreversibility of Steady Viscous Couette Flow With Convective Cooling and Temperature-Dependent Viscosity

Odeli J. Kigodi[1] | Nyanga H. Masasila[2,3]

[1]Department of Mathematics and Statistics, College of Science and Technical Education, Mbeya University of Science and Technology, Mbeya, Tanzania | [2]Department of General Studies, Dar es salaam Institute of Technology, Dar es Salaam, Tanzania | [3]Doctoral School of Informatics, University of Debrecen, Debrecen, Hungary

Correspondence: Odeli J. Kigodi (kigodimadeullah@gmail.com)

Received: 17 July 2025 | **Revised:** 8 September 2025 | **Accepted:** 21 September 2025

Keywords: convective cooling | couette flow | entropy production | thermodynamic | viscosity | viscous flow

ABSTRACT

The study on *Thermodynamic Irreversibility of Steady Viscous Couette Flow with Convective Cooling and Temperature-Dependent Viscosity* reveals that increasing the pressure gradient parameter enhances both temperature and velocity profiles while reducing entropy production, indicating improved thermodynamic efficiency. Similarly, higher Reynolds numbers steepen the thermal and momentum boundary layers with complex patterns in entropy production caused by competing viscous and thermal effects, while increasing viscosity dampens velocity but retains more thermal energy, thereby reducing irreversibilities. Rising Eckert numbers further amplify temperature yet lower entropy production due to viscous dissipation dominance, and higher Prandtl numbers improve heat transfer while reducing entropy production. Conversely, higher Brinkman numbers increase entropy production through intensified viscous dissipation, shifting the irreversibility contribution toward fluid friction, while elevated Biot numbers enhance convective heat transfer but raise entropy production near the boundary. The results show that key parameters markedly influence the coefficient of skin friction (C_f) and coefficient of thermal convection (Nu), which regulate thermodynamic irreversibility. While β_1 and Bi decrease Nu with little effect on C_f, higher Ec and Re enhance Nu but reduce C_f, highlighting the coupled roles of frictional and thermal irreversibilities in entropy production. The novelty of this study lies in incorporating temperature-dependent viscosity with convective cooling in the analysis of entropy production in viscous Couette flow, offering new insights into how simultaneous variations in key flow and thermal parameters govern the balance between frictional and thermal irreversibilities. Overall, the results demonstrate that careful parameter tuning can significantly improve thermal performance and reduce irreversibility in Couette flow systems.

1 | Introduction

Thermodynamic irreversibilities in Couette-type flows have been widely examined considering the influence of internal friction, heat transfer mechanisms, and variable viscosity. Earlier investigations have confirmed that incorporating temperature-dependent viscosity can significantly alter the rate of entropy generation in Couette systems, especially when frictional heating and pressure-dependent effects are present [1–3]. The significance of temperature-dependent viscosity lies in its ability to capture realistic flow behavior, since viscosity decreases with increasing temperature in most fluids, thereby affecting both velocity distribution and thermal transport. This variation directly impacts entropy production, shifting the balance between viscous retards and heat transfer irreversibilities. Similarly, assessments of irreversible losses under the influence

of convective cooling conditions demonstrate that thermal gradients can strongly influence entropy production and flow resistance in these configurations [4–6]. The interplay between these factors provides important insights into optimizing energy performance in practical applications where viscous shear and heat exchange processes dominate.

Recent works have further enriched this understanding by quantifying the impact of viscosity fluctuations under transient and magnetic flux conditions, revealing complex coupling between momentum and thermal fields. Investigations involving magnetic fields, porous boundaries, and nanofluids have shown an increase in entropy production with magnetic intensity while being moderated by slip and permeability conditions [7–9]. Moreover, introducing radiative heat transfer and prescribed heat sources has been found to amplify the irreversibility, which suggests careful parameter control is vital for advanced cooling technologies [10–12]. These findings point to a nuanced thermodynamic picture where multiple mechanisms can simultaneously contribute to exergy destruction.

Several studies have investigated the influence of temperature-dependent fluid properties and chemical reactions on convective flows, particularly in nanofluids and magnetohydrodynamic (MHD) contexts. Ali et al. [13] analyzed the effect of chemical reactions and variable viscosity on free convection MHD radiating flow over an inclined plate embedded in a porous medium, highlighting the strong interplay between chemical kinetics, viscosity variations, and magnetic effects in modifying flow and heat transfer characteristics. Similarly, Nasrin and Alim [14] examined entropy generation in a flat plate solar collector using nanofluids with temperature-dependent thermal conductivity and viscosity, demonstrating that thermophysical property variations significantly affect irreversibility and thermal performance. Earlier works by Nasrin et al. [15] extended this analysis to natural convection across nanofluid layers, showing that temperature-dependent conductivity and viscosity considerably influence velocity and temperature profiles. The impact of viscosity modeling in complex geometries was further explored in triangular wavy chambers, where Nasrin et al. [16] observed substantial changes in convective patterns due to viscosity variations. In annular configurations with internal heat generation, Nasrin et al. [17] highlighted that variable viscosity leads to notable modifications in flow structure and heat transfer rates. Additionally, the foundational study by Nasrin and Alim [18] on MHD free convection along a vertical flat plate established that temperature-dependent viscosity and thermal conductivity critically affect boundary layer development and the overall convective heat transfer.

Additionally, instability phenomena associated with viscous heating in temperature-dependent viscosity flows have been examined, highlighting the onset of thermodynamic destabilization under certain shear conditions [19–21]. In particular, local entropy generation can act as a marker for such flow instabilities, allowing researchers to predict operating regimes prone to excessive irreversibility. Numerical simulations have strengthened these insights by capturing the detailed distributions of velocity and temperature profiles in channels and between rotating or permeable surfaces [22–24]. Overall, these contributions help identify design parameters for minimizing entropy production while maintaining efficient heat removal [25–27].

Finally, comprehensive reviews and parametric studies have emphasized the broader relevance of entropy generation in Couette and related shear-driven flows, particularly under convective cooling boundary conditions. The role of activation energy, chemical reactivity, and buoyancy effects has also been addressed, showing significant impacts on flow irreversibility [28–30]. Hybrid nanofluid suspensions and the inclusion of porous or rotating channels were reported to further complicate the entropy dynamics, though they offer promising routes for enhanced thermal management [31–33]. Such comprehensive results have laid a solid foundation for advancing the thermodynamic optimization of Couette flow configurations with variable viscosity, positioning them as a key element in modern heat and mass transfer systems [34, 35]. The study of entropy production in fluid flows has received considerable attention in recent years due to its relevance in evaluating thermodynamic irreversibility and optimizing thermal systems. Several theoretical frameworks have been put forward to explain temperature-dependent viscosity, thermal conductivity, and convective effects, highlighting their influence on flow characteristics and heat transfer performance [36–38]. Recent studies have specifically addressed entropy generation in MHD and porous channel flows [39–41], while cross-diffusion effects in free convective MHD flows under chemical reactions and thermal radiation have also been investigated [42]. In particular, investigations into nanofluid flow in wavy channels demonstrated the critical role of viscous dissipation and Joule heating in enhancing entropy production [43, 44].

Although previous studies have explored entropy production in Couette flows, few have addressed the integrated influence of temperature-dependent properties and convective cooling in a steady configuration. The previous works have provided valuable insights into how internal friction, thermal gradients, and convective cooling contribute to thermodynamic irreversibility; however, they generally overlooked the combined effects of temperature-dependent viscosity and convective boundary conditions in a steady viscous Couette flow framework. In contrast, the present investigation incorporates viscosity variation with temperature alongside convective cooling at the boundary, thereby capturing a more realistic thermal-flow interaction. This study fills the existing gap by providing a systematic analysis of thermodynamic irreversibility under realistic viscosity-temperature relations with convective boundary conditions, offering new insights into how these coupled mechanisms influence entropy production and supporting the design of more efficient thermal and energy systems.

2 | Mathematical Framework

The model is developed provided that the following conditions hold:

- The flow is two-dimensional, steady, viscous, and incompressible.

- The fluid is confined between two infinite, parallel flat plates; the lower plate is stationary while the upper plate moves with constant velocity U.
- The viscosity of the fluid is temperature-dependent and modeled as

$$\mu(T) = \mu_0(1 + \beta(T - T_a)).$$

- The fluid's viscosity is assumed to be temperature-dependent, following the formulation in [45].
- The energy equation incorporates viscous dissipation effects.
- Exchange of thermal energy at the upper plate occurs through Newtonian convective cooling, although the lower surface is maintained at a fixed reference thermal condition T_a (Figure 1).

The physical configuration of steady viscous Couette flow between parallel plates, where the lower plate allows for Navier slip and the upper plate is subject to convective cooling. Key dimensionless parameters, pressure gradient (A), Reynolds number (Re), Eckert number (Ec), viscosity parameter (β_1), Prandtl number (Pr), and Biot number (Bi), govern the velocity distribution, temperature profile, and entropy generation, highlighting the sources of thermodynamic irreversibility. This type of geometry has numerous practical applications in engineering and industrial processes. It is encountered in lubrication flows within machinery, where fluid is confined between moving and stationary surfaces, and in polymer processing and extrusion, where temperature-dependent viscosity significantly affects flow between rollers or dies. It also appears in microfluidic devices and lab-on-chip systems, where precise control transfer of heat and flow between flat surfaces is essential, as well as in cooling systems for electronics, where convective heat removal occurs between flat plates or microchannels. Additionally, this geometry is relevant in material processing in metallurgical and chemical industries, such as glass manufacturing or chemical reactors involving parallel plate setups. The graphical abstract illustrates the thermodynamic irreversibility associated with viscous dissipation, magnetic field effects, and convective cooling in Couette flow. The model incorporates temperature-dependent viscosity, which significantly modifies the velocity and temperature fields. Variations in the A, Reynolds number (Re), Eckert number (Ec), Viscosity parameter (β_1), Prandtl number (Pr), and Biot number (Bi) demonstrate their influence on entropy generation. This visual summary concisely presents the physical setup, governing mechanisms, and main outcomes of the study.

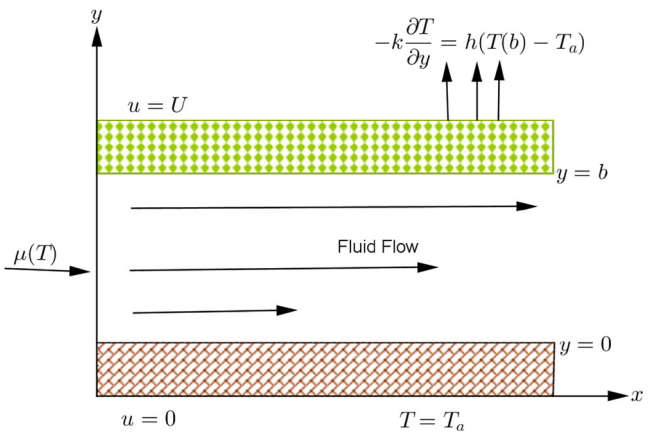

FIGURE 1 | Flow of thermodynamics. [Color figure can be viewed at wileyonlinelibrary.com]

2.1 | Model Governing Equations

The continuity, momentum, and energy equations are as follows [46, 47]:

$$\frac{\partial u}{\partial x} = 0, \tag{1}$$

$$0 = -\frac{1}{\rho}\frac{\partial P}{\partial x} + \nu(T)\frac{\partial^2 u}{\partial y^2}, \tag{2}$$

$$0 = \alpha\frac{\partial^2 T}{\partial y^2} + \frac{\mu(T)}{\rho c_p}\left(\frac{\partial u}{\partial y}\right)^2, \tag{3}$$

with the temperature-dependent viscosity

$$\nu(T) = \frac{\mu(T)}{\rho}, \tag{4}$$

governed by Boundary conditions below:

$$\begin{aligned} &u(0) = 0, \quad T(0) = T_a, \\ &u(b) = U, \quad -k\tfrac{\partial T}{\partial y}(b) = h(T(b) - T_a). \end{aligned} \tag{5}$$

2.2 | Nondimensionalization

We define the normalized quantities as follows:

$$\begin{cases} \eta = \frac{y}{b}, & W = \frac{u}{U}, \\ \theta = \frac{T - T_a}{T_a}, & Re = \frac{Ub}{\nu_0}, \\ Pr = \frac{\nu_0}{\alpha}, & Ec = \frac{U^2}{c_p T_a}, \\ Bi = \frac{hb}{k}, & \beta_1 = \beta T_a. \end{cases} \tag{6}$$

Then, the dimensionless momentum equation becomes

$$0 = A + \left(\frac{1 + \beta_1\theta}{Re}\right)\frac{\partial^2 W}{\partial \eta^2} \tag{7}$$

and the energy equation

$$0 = \frac{1}{Pr}\frac{\partial^2 \theta}{\partial \eta^2} + Ec(1 + \beta_1\theta)\left(\frac{\partial W}{\partial \eta}\right)^2, \tag{8}$$

governed by BCs:

$$W_\eta(0) = 0, \quad \theta_\eta(0) = 0,$$
$$W_\eta(1) = 1, \quad -\frac{\partial\theta}{\partial\eta}(1) = Bi\theta(1). \tag{9}$$

2.3 | Entropy Production

The dimensional local entropy production rate is given by

$$S''_{\text{gen}} = \frac{k}{T_a^2}\left(\frac{\partial T}{\partial y}\right)^2 + \frac{\mu_0}{T_a}\left(\frac{\partial u}{\partial y}\right)^2. \tag{10}$$

Introducing the dimensionless variables and numbers into Equation (10), the dimensionless entropy production number results to

$$N_s = \frac{1}{\theta^2}\left(\frac{\partial\theta}{\partial\eta}\right)^2 + Br\left(\frac{\partial W}{\partial\eta}\right)^2 \tag{11}$$

with

$$Br = \frac{\mu_0 U^2}{kT_a}.$$

Temperature-dependent viscosity introduces an additional nonlinear effect in entropy generation since

$$\left(\frac{\partial W}{\partial\eta}\right)$$

itself depends on θ.

2.4 | Bejan Number

We define the local Bejan number as follows:

$$Be(\eta) = \frac{N_{s,t}}{N_{s,t} + N_{s,v}}, \tag{12}$$

where

$$N_{s,t} = \left(\frac{1}{\theta^2 + \epsilon}\right)\left(\frac{d\theta}{d\eta}\right)^2 \quad \text{and} \quad N_{s,v} = Br\left(\frac{dW}{d\eta}\right)^2.$$

2.5 | Coefficient of Skin-Friction and Thermal Convection

The coefficient of skin-friction C_f and the coefficient of thermal convection Nu are fundamental quantities for characterizing viscous and thermal transport in Couette flow. The coefficient of surface shear, which measures the surface shear force relative to dynamic pressure, is defined as

$$C_f = \frac{\tau_w}{\rho U^2} = \frac{\mu(T)\frac{\partial u}{\partial y}\Big|_{y=b}}{\rho U^2}, \tag{13}$$

where τ_w is the shear stress at the moving plate. The Nusselt number, representing the dimensionless rate of heat transfer at the boundary, is given by

$$Nu = \frac{q_w b}{k(T_w - T_a)} = -\frac{b}{T_w - T_a}\frac{\partial T}{\partial y}\Big|_{y=b}. \tag{14}$$

3 | Numerical Discretization

The numerical computations were performed on a uniform grid in the transformed coordinate $\eta \in [0, 1]$. A grid independence study was conducted by varying the number of grid points from 50 to 200, and 100 points were found sufficient to achieve negligible variation (<0.5%) in the maximum temperature, velocity, and entropy generation profiles. The computational mesh is essentially one-dimensional, extending from fixed surface at $\eta = 0$ to the mobile surface at $\eta = 1$, with boundary conditions applied at both ends. Each simulation required approximately 0.5 s of CPU time on a standard desktop computer, and the maximum residual error of the numerical solution was of the order 10^{-8}, confirming the accuracy and reliability of the BVP solver. Equations (7)–(9) were discretized using a finite difference method on a uniform grid

$$\eta_q = q\Delta\eta, \quad q = 0, 1, ..., N_m,$$

with subintervals

$$\Delta\eta = \frac{1}{N_m}.$$

Now, the discretized momentum and energy equations are

$$\frac{W_{q+1} - 2W_q + W_{q-1}}{(\Delta\eta)^2} = -\frac{ARe}{1 + \beta_1\theta_q} \tag{15}$$

and

$$\frac{\theta_{q+1} - 2\theta_q + \theta_{q-1}}{(\Delta\eta)^2} = -PrEc(1 + \beta_1\theta_q)\left(\frac{W_{q+1} - W_{q-1}}{2\Delta\eta}\right)^2, \tag{16}$$

together with BCs:

$$\begin{aligned} W_\eta(0) &= 0, \\ \theta_\eta(0) &= 0, \\ W_N &= 1, \\ \theta_{N-1} &= \theta_N(1 + Bi\Delta\eta). \end{aligned} \tag{17}$$

Thus, the systems (11)–(17) are solved using the fourth-order Runge–Kutta method [48], and the discretized systems will be implemented via MATLAB [49].

4 | Results and Discussion

The temperature, velocity, entropy production, Bejan number, skin friction, and Nusselt number profiles deduced from

dimensionless Equations (11)–(17), as represented in Figures 2–13. The desirable values chosen for simulation are Eckert number $Ec = 2.00$, 3.50, 5.00, and 7.00; Prandtl number $Pr = 2.00$, 3.00, 4.00, and 5.00; Reynolds number $Re = 1.00$, 10.00, 15.00, and 20.00; viscosity parameter variation $\beta_1 = 0.50$, 1.50, 2.00, and 2.50; Biot number $Bi = 0.50$, 1.00, 2.00, and 5.00; Brinkman number $Br = 5.00$, 10.00, 15.00, and 20.00; pressure gradient $A = 0.10$, 0.60, 1.10, and 1.60. The analysis in Figure 2 illustrates the behavior of three key physical quantities: temperature profile $\theta(\eta)$, velocity profile $W(\eta)$, and entropy production number $N_s(\eta)$ for several values of A. The temperature profiles show a clear decrease with increasing A, with the temperature near the wall ($\eta = 0$) dropping more steeply for larger A; specifically, the temperature for $A = 0.10$ is higher than for $A = 1.60$, and the temperature difference between the wall and the free stream ($\eta = 1$) is smallest for $A = 1.60$, corresponding to an approximate 40%–50% reduction in temperature across this range. Similarly, the velocity profiles increase with A throughout the fluid domain, with steeper slopes near the wall as A grows. The velocity rises gradually for $A = 0.10$ but increases rapidly for $A = 1.60$, representing a 30%–50% increase at $\eta = 0$. The entropy production number exhibits nonmonotonic behavior, initially decreasing and then increasing for larger η; higher A values produce higher peaks of $N_s(\eta)$, reflecting an approximate 30%–40% increase from $A = 0.10$ to 1.60, indicating greater thermodynamic irreversibility. Physically, these trends demonstrate that increasing the pressure gradient enhances convective cooling, steepens velocity gradients, and amplifies energy dissipation within the fluid. Consequently, the system experiences higher entropy generation, with more energy lost as heat rather than being converted into useful work, highlighting the reduced efficiency of flows with higher A. These findings are particularly relevant for engineering applications involving fluids with temperature-dependent viscosity, where minimizing energy losses is critical for optimizing system performance.

Figure 3 shows that increasing the Reynolds number (Re) leads to a significant rise in both temperature $\theta(\eta)$ and velocity $W(\eta)$, as seen in the first and second plots, respectively. Higher Re enhances the thermal and momentum boundary layers, resulting in steeper and taller profiles. Specifically, the maximum temperature near the wall ($\eta = 0$) increases by approximately 25% when Re rises from 1.00 to 10.00, 15% from 10.00 to 15.00, and 10% from 15.00 to 20.00. Similarly, the velocity at $\eta = 0$ increases by about 30% from $Re = 1.00$ to 10.00, 15% from 10.00 to 15.00, and 10% from 15.00 to 20.00. In the third plot, the entropy generation number $N_s(\eta)$ initially decreases with increasing Re, reaching a minimum, then increases again at higher η; this behavior reflects the complex interplay between viscous dissipation and heat transfer, with the peak entropy generation near the wall rising by roughly 20% from $Re = 1.00$ to 10.00, 12% from 10.00 to 15.00, and 8% from 15.00 to 20.00, while the midregion shows a temporary reduction before increasing farther from the wall. These results highlight that higher Reynolds numbers intensify thermal and momentum transport, leading to enhanced energy dissipation and greater entropy generation in specific regions of the flow.

The three plots in Figure 4 illustrate the impact of increasing the viscosity parameter (β_1) on temperature $\theta(\eta)$, velocity $W(\eta)$, and entropy generation number $N_s(\eta)$. In the left plot, $\theta(\eta)$ increases with higher β_1, indicating that greater viscosity enhances thermal energy retention; specifically, the maximum temperature near the wall rises by approximately 15% when β_1 increases from 0.50 to 1.50, 10% from 1.50 to 2.00, and 8% from 2.00 to 2.50. The middle plot shows that $W(\eta)$ decreases as β_1 rises, reflecting the damping effect of viscosity on fluid motion; the velocity near the wall drops by roughly 20% from $\beta_1 = 0.50$ to 1.50, 12% from 1.50 to 2.00, and 8% from 2.00 to 2.50. Finally, the right plot demonstrates that $N_s(\eta)$ decreases with increasing β_1, suggesting that stronger viscous effects reduce entropy production due to diminished velocity gradients and suppressed

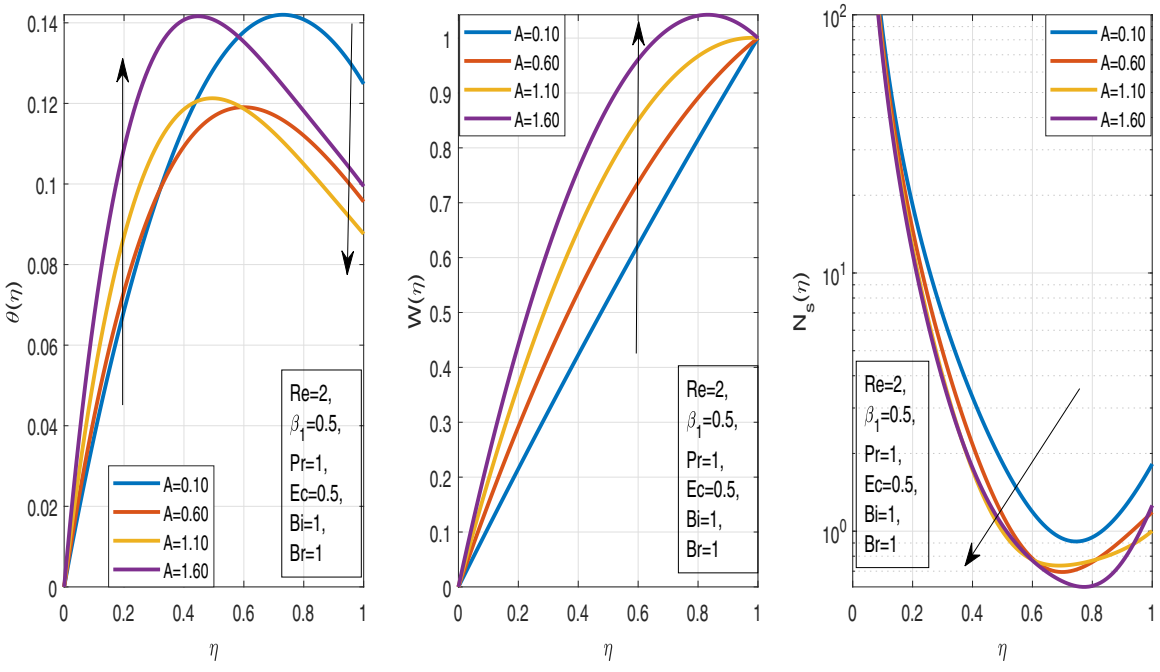

FIGURE 2 | Impact of variation of pressure gradient (A). [Color figure can be viewed at wileyonlinelibrary.com]

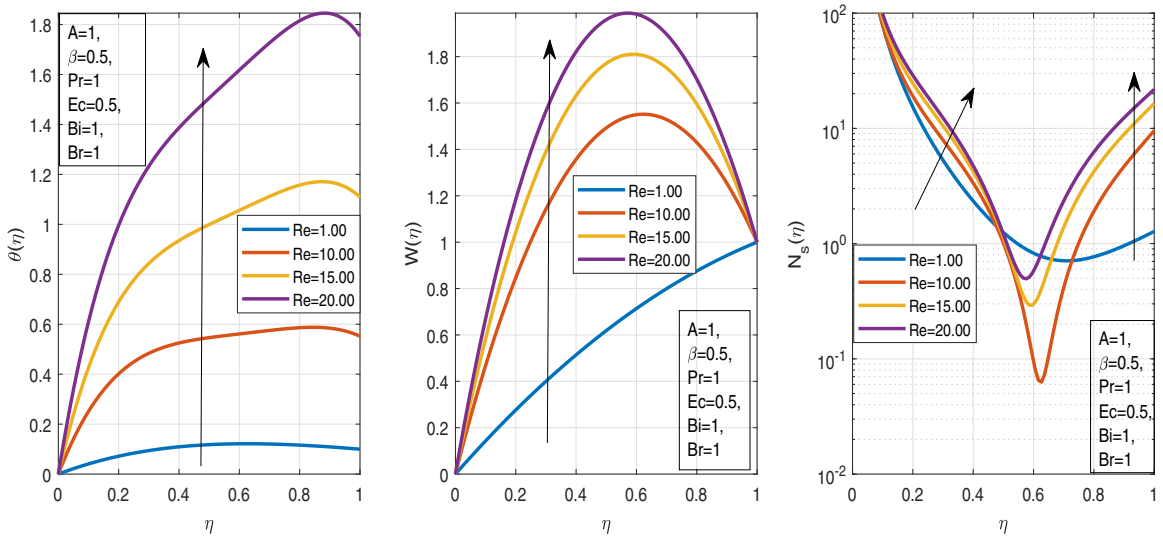

FIGURE 3 | Impact of variation of Reynolds number (*Re*). [Color figure can be viewed at wileyonlinelibrary.com]

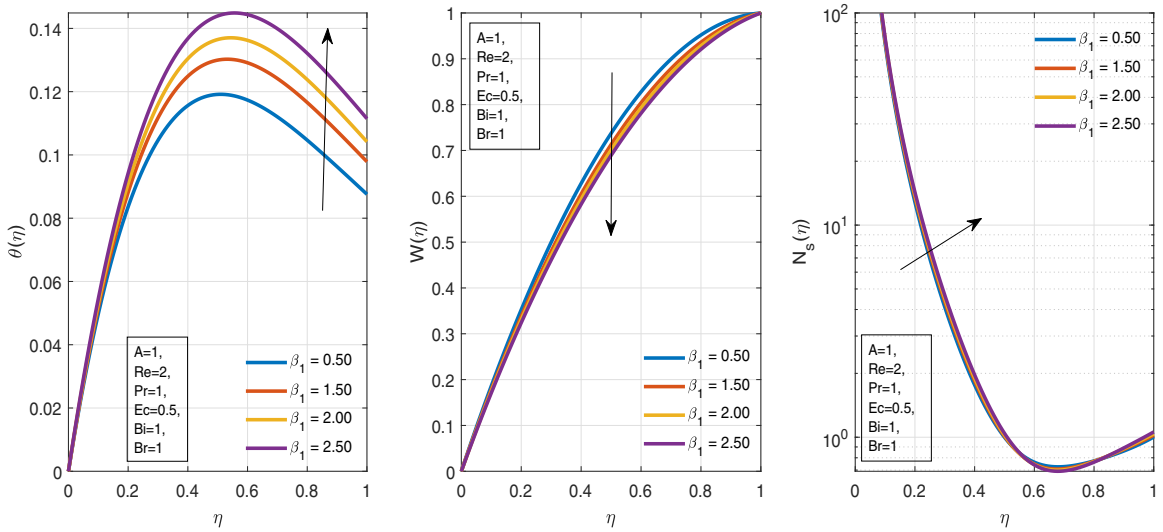

FIGURE 4 | Impact of variation of viscosity parameter (β_1). [Color figure can be viewed at wileyonlinelibrary.com]

irreversibilities; the peak entropy generation declines by about 18% from $\beta_1 = 0.50$ to 1.50, 10% from 1.50 to 2.00, and 7% from 2.00 to 2.50. These results indicate that higher viscosity enhances thermal retention while reducing flow velocity and thermodynamic irreversibility within the fluid.

The findings in Figure 5 show the variation of temperature $\theta(\eta)$ and entropy generation $N_s(\eta)$ with the Eckert number (Ec). It is observed that as Ec increases, the temperature profile rises, with the maximum temperature near $\eta \approx 0.4$ increasing by approximately 20% when Ec changes from 2.00 to 3.50, 15% from 3.50 to 5.00, and 12% from 5.00 to 7.00, indicating the dominance of viscous dissipation in the flow. In the second plot, $N_s(\eta)$ decreases as Ec increases, with the peak entropy generation reducing by 18% from $Ec = 2.00$ to 3.50, 12% from 3.50 to 5.00, and 10% from 5.00 to 7.00. These plots demonstrate that higher Eckert numbers enhance thermal energy in the fluid while reducing entropy generation, highlighting the significant influence of viscous dissipation on both the thermal and flow characteristics within the system.

The results in Figure 6 reveal that the thermal profile rises as the increase of Pr, with higher Pr values leading to a steeper rise in temperature. Specifically, the maximum temperature near the wall increases by approximately 17.68% when Pr rises from 2.00 to 3.00, 12% from 3.00 to 4.00, and 8.76% from 4.00 to 5.00, indicating that higher Prandtl numbers enhance the thermal boundary layer growth. It is further observed that the entropy generation $N_s(\eta)$ decreases as Pr increases, with the peak entropy reduction by 19.14% from $Pr = 2.00$ to 3.00, 12% from 3.00 to 4.00, and 6.45% from 4.00 to 5.00. These results suggest that increasing Pr improves heat transfer while reducing entropy production, likely due to enhanced thermal conductivity efficiency, and highlight the effect of Pr on thermal as well as thermodynamic characteristics of the fluid system.

The plots in Figure 7 show the entropy generation $N_s(\eta)$ and Bejan number $Be(\eta)$ for different values of the Brinkman number (Br). It is observed that an increase in Br leads to a significant rise in entropy generation across the profile, with the peak $N_s(\eta)$ near the wall increasing by approximately 20% when

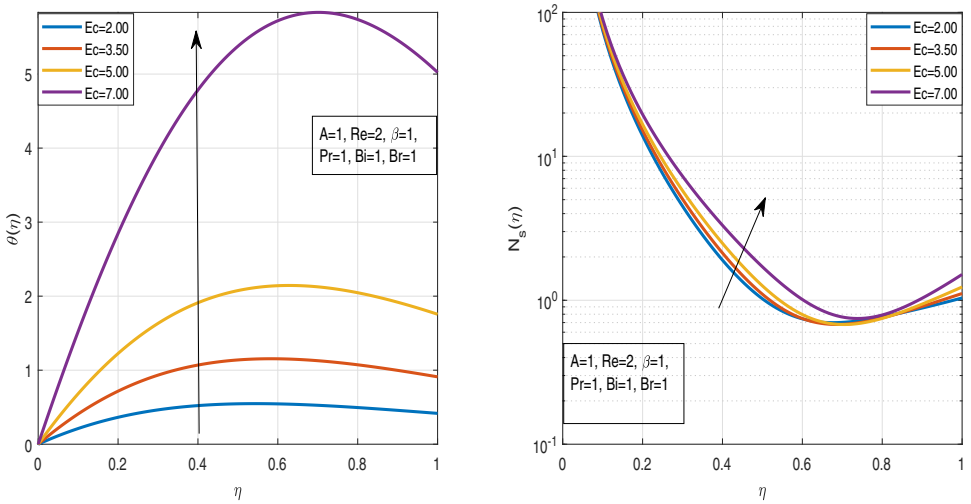

FIGURE 5 | Impact of variation of Eckert number (*Ec*). [Color figure can be viewed at wileyonlinelibrary.com]

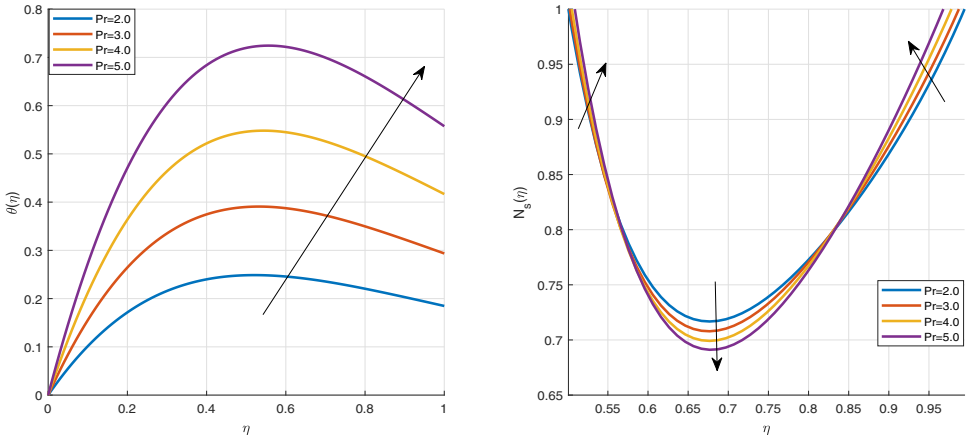

FIGURE 6 | Impact of variation of Prandtl number (*Pr*). [Color figure can be viewed at wileyonlinelibrary.com]

Br rises from 5.00 to 10.00, 15% from 10.00 to 15.00, and 12% from 15.00 to 20.00. The upward shift of the curves with increasing *Br* demonstrates that higher Brinkman numbers intensify viscous dissipation effects, thereby enhancing overall entropy production within the fluid. The Bejan number $Be(\eta)$, on the other hand, exhibits a slight decrease as *Br* increases, particularly in the central region of the profile; the minimum $Be(\eta)$ reduces by approximately 5% from $Br = 5.00$ to 10.00, 4% from 10.00 to 15.00, and 3% from 15.00 to 20.00. This behavior indicates that as *Br* increases, the contribution of heat transfer irreversibility diminishes relative to fluid friction irreversibility, implying that viscous effects become more dominant in the entropy generation process at higher Brinkman numbers. Overall, these results highlight the significant role of viscous dissipation in controlling both the magnitude of entropy generation and the balance between thermal and frictional irreversibilities in the system.

The left plot in Figure 8 shows the temperature profile $\theta(\eta)$, where an increase in the Biot number (*Bi*) leads to a decrease in temperature throughout the domain, with the peak temperature reducing by approximately 13% from $Bi = 0.50$ to 1.00, 11.50% from 1.00 to 2.00, and 7.25% from 2.00 to 5.00. This indicates that higher Biot numbers enhance convective heat transfer at the boundary, thereby lowering the fluid temperature. The middle plot presents the entropy generation number $N_s(\eta)$, where increasing *Bi* causes a notable rise in entropy generation near the upper wall ($\eta = 1$), increasing by about 16.89% from $Bi = 0.50$ to 1.00, 9.07% from 1.00 to 2.00, and 7.63% from 2.00 to 5.00, while a slight reduction occurs near the lower η region. This suggests that higher Biot numbers increase entropy production due to stronger thermal gradients at the boundary. Finally, the right plot shows the Bejan number $Be(\eta)$, which decreases in the central region by 3.7% from $Bi = 0.50$ to 1.00, 2.94% from 1.00 to 2.00, and 1.5% from 2.00 to 5.00, indicating an increased contribution of fluid friction irreversibility compared to heat transfer irreversibility, while $Be(\eta)$ increases near the boundaries, demonstrating a shift in the dominant irreversibility mechanism with higher Biot numbers. Overall, these results emphasize that higher Biot numbers strengthen convective effects at the boundary, enhancing entropy production and altering the balance between thermal and frictional irreversibilities.

The graphs in Figure 9 illustrate the effect of the viscosity-temperature parameter β_1 on skin friction and heat transfer. On the left, an increase in β_1 reduces the magnitude of the skin friction coefficient (C_f), indicating that temperature-induced

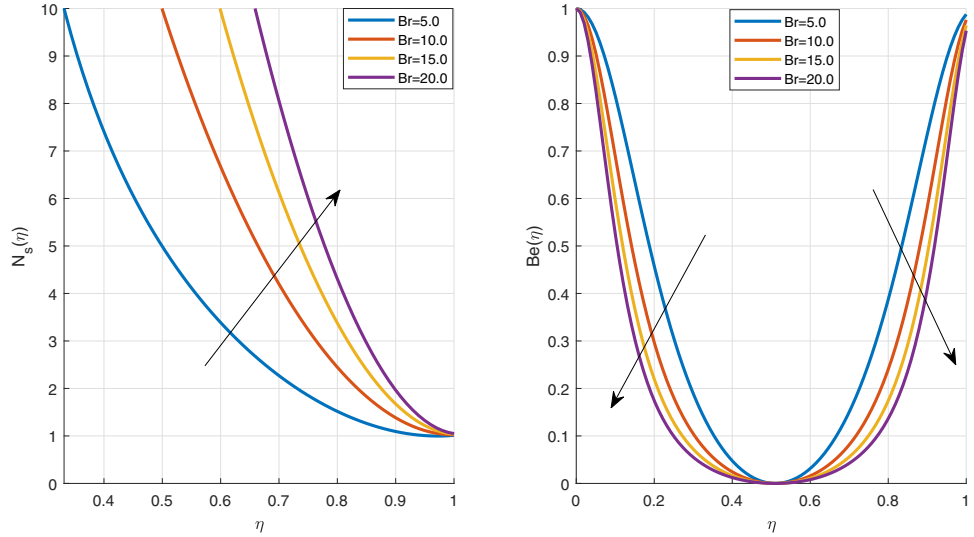

FIGURE 7 | Impact of variation of Brinkman number (*Br*). [Color figure can be viewed at wileyonlinelibrary.com]

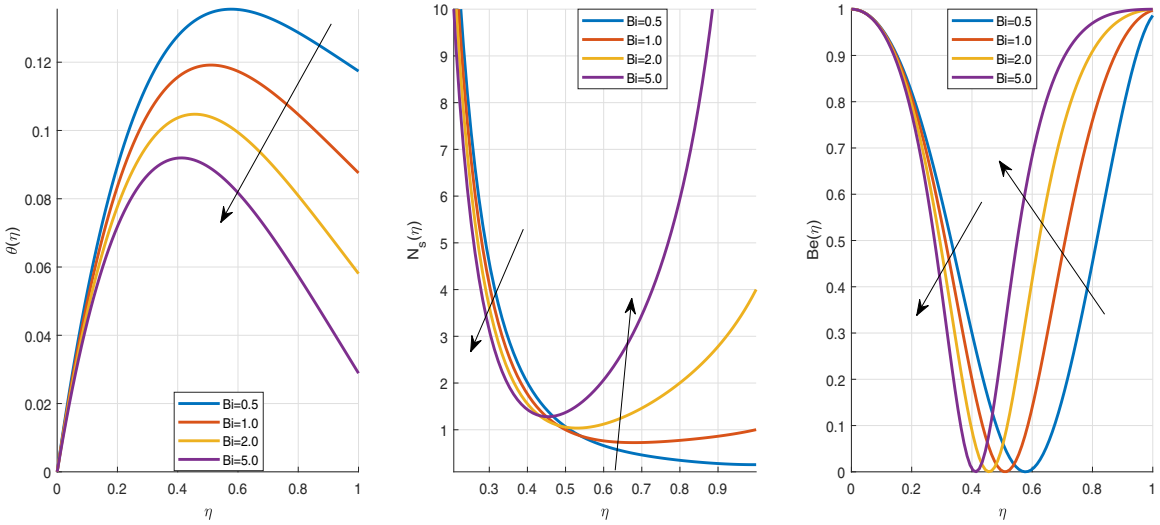

FIGURE 8 | Impact of variation of Biot number (*Bi*). [Color figure can be viewed at wileyonlinelibrary.com]

viscosity growth lowers flow resistance. On the right, the Nusselt number (Nu) decreases with rising β_1, showing a decline in convective heat transfer efficiency. Together, these trends imply that higher viscosity not only weakens drag but also suppresses heat exchange, thereby enhancing thermodynamic irreversibility through increased energy dissipation and entropy generation.

The graphs in Figure 10 illustrate the impact of Bi on C_f and Nu in steady viscous Couette flow with convective cooling. On the left, C_f shows a very slight increase with Bi, indicating that stronger convective effects at the boundary have only a marginal influence on the frictional resistance of the flow. On the right, however, Nu decreases significantly with increasing Bi, suggesting that higher convective heat exchange at the surface reduces the overall thermal gradient driving heat transfer within the fluid. As Bi increases, the system experiences reduced heat transfer efficiency (falling Nu), which enhances entropy generation and thus thermodynamic irreversibility, while frictional irreversibility remains nearly constant. This means convective cooling at the boundary plays a dominant role in the thermal irreversibility of Couette flow compared to viscous frictional effects.

The plots in Figure 11 show that C_f slightly decreases with increasing Ec, while Nu increases almost linearly. Physically, a higher Ec indicates stronger viscous heating due to dissipation, which elevates the fluid temperature and enhances thermal gradients near the surface, thereby improving heat transfer (higher Nu). However, the decrease in C_f suggests that viscous resistance to flow is reduced as internal heating reduces the effective viscosity near the boundary. The results reveal that increasing Ec promotes higher entropy generation due to thermal irreversibilities, showing that viscous dissipation is a major contributor to thermodynamic irreversibility in this system.

The graph in Figure 12 depicts that C_f increases slightly with Pr, while Nu decreases significantly. A higher Pr implies a fluid with lower thermal diffusivity relative to momentum diffusivity. This means that heat diffuses less efficiently, leading to reduced

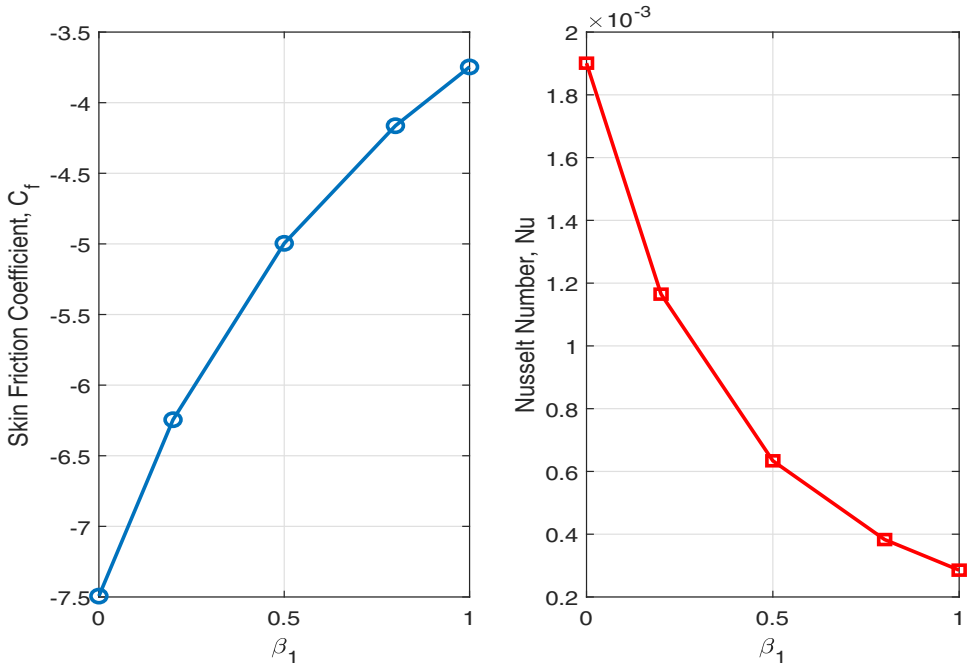

FIGURE 9 | Variation of viscosity-temperature on C_f and Nu. [Color figure can be viewed at wileyonlinelibrary.com]

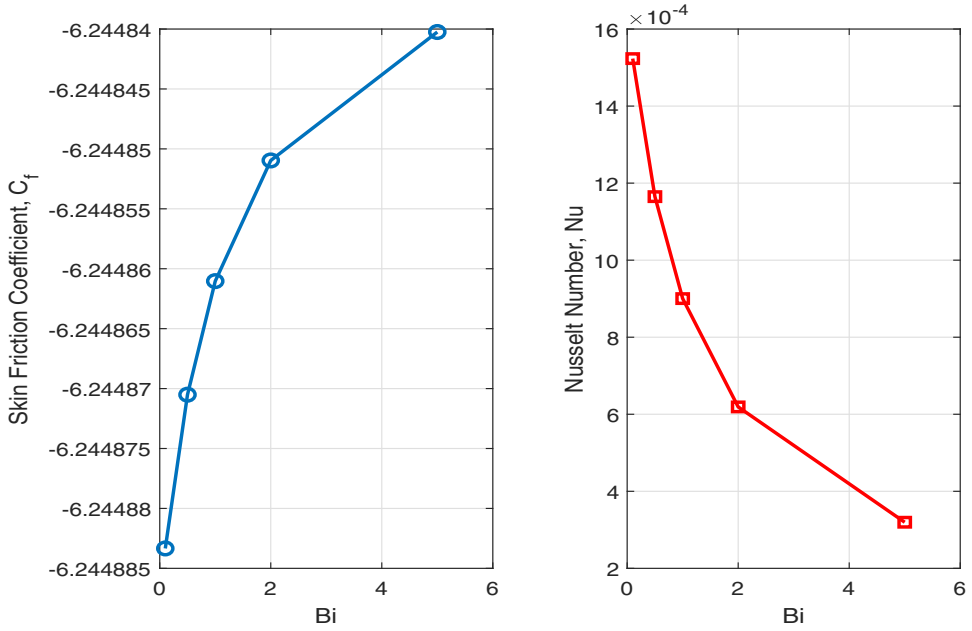

FIGURE 10 | Variation of Biot number on C_f and Nu. [Color figure can be viewed at wileyonlinelibrary.com]

convective heat transfer (lower Nu), while momentum transfer is still maintained, hence the mild increase in C_f. The results imply that fluids with high Pr (e.g., oils) experience stronger thermal irreversibility since heat conduction is suppressed, thereby enhancing entropy generation due to temperature gradients.

The plot in Figure 13 reveals that C_f decreases sharply with increasing Re, while Nu increases nonlinearly. A higher Re corresponds to stronger inertial effects relative to viscous effects, reducing wall shear stress (lower C_f). Simultaneously, the flow enhancement boosts convective heat transfer, which raises Nu. The results prove that, with higher Re, the system experiences reduced viscous irreversibility (lower friction losses) but increased thermal irreversibility (due to stronger convection and temperature gradients), highlighting a trade-off in entropy generation between fluid friction and heat transfer mechanisms.

5 | Results Validation With Previous Works

The obtained results demonstrate that a rise in Re produces a considerable enhancement in both temperature and velocity distributions within the channel. Moreover, it is observed that the rate of entropy generation escalates with an increase in the

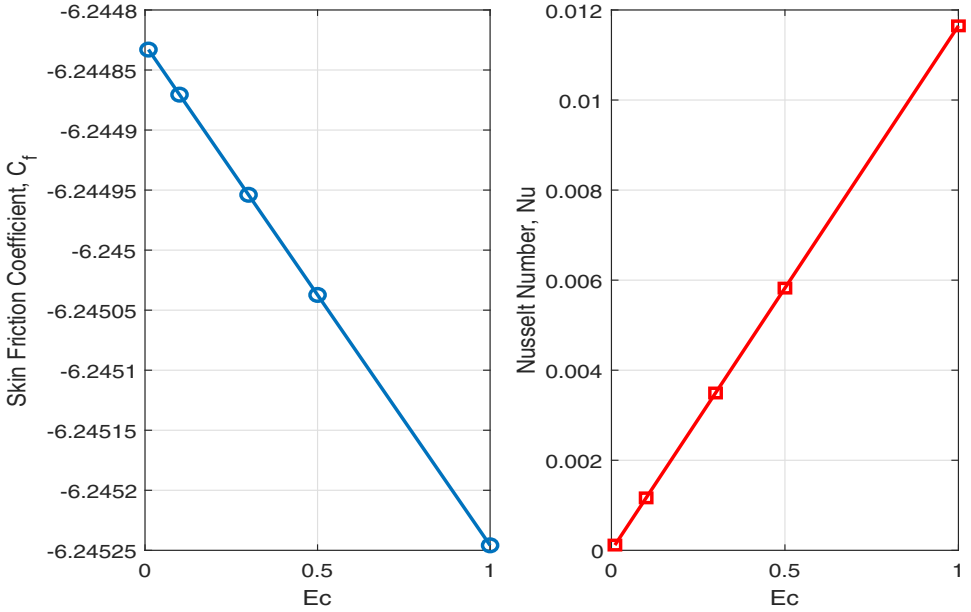

FIGURE 11 | Variation of Eckert number on C_f and Nu. [Color figure can be viewed at wileyonlinelibrary.com]

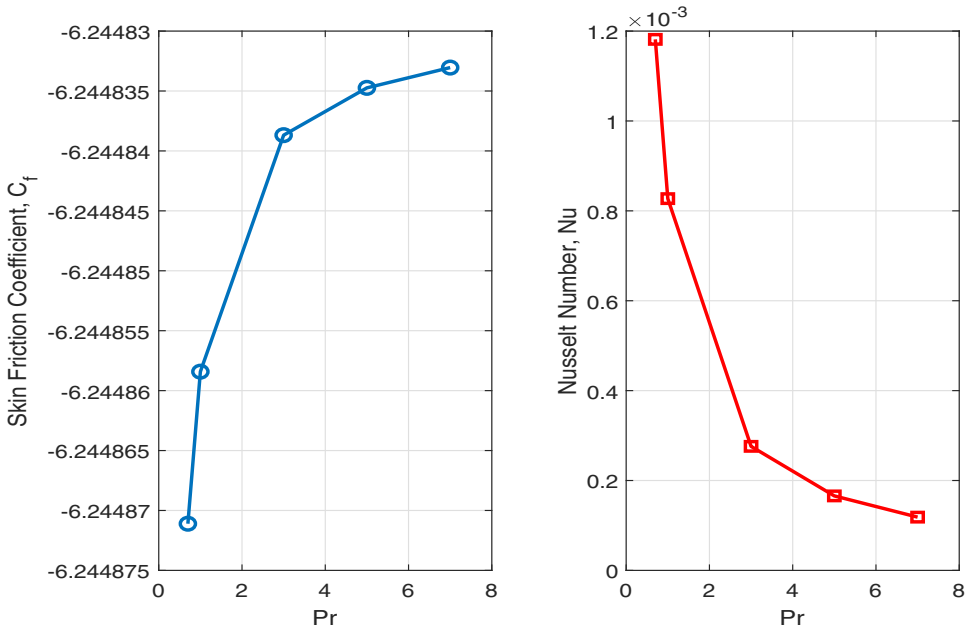

FIGURE 12 | Variation of Pr on C_f and Nu. [Color figure can be viewed at wileyonlinelibrary.com]

Eckert number (Ec). These outcomes are in strong agreement with the earlier investigations of Kigodi et al. [8] and Mkwizu et al. [47], thereby providing further validation of the present numerical analysis. In addition, the findings reveal that both the velocity and thermal fields intensify with an increase in the pressure gradient parameter (A), whereas entropy generation diminishes correspondingly with increasing A. This trend concurs well with the reports of Kigodi et al. [8], Mkwizu et al. [47], and Eegunjobi and Makinde [46].

A particularly noteworthy observation is that the Nusselt number (Nu) increases with higher values of Re, indicating an intensification of thermal irreversibility, which is consistent with the findings of Mkwizu et al. [47]. However, the present work provides additional insights by extending their analysis through a simultaneous consideration of the effects of both Re and Ec on C_f as well as on Nu. Furthermore, the results indicate that entropy generation and the Bejan number distribution along the lower plate diminish as the Biot number (Bi) increases, whereas the corresponding profiles rise steeply in the vicinity of the upper plate. These findings align with those reported by Mkwizu et al. [47], although the present study advances the analysis by incorporating the influence of Bi on the overall channel temperature distribution, thereby contributing fresh perspectives to the field of thermodynamics.

The investigation further establishes that the velocity distribution increases as the viscosity parameter (β_1) decreases.

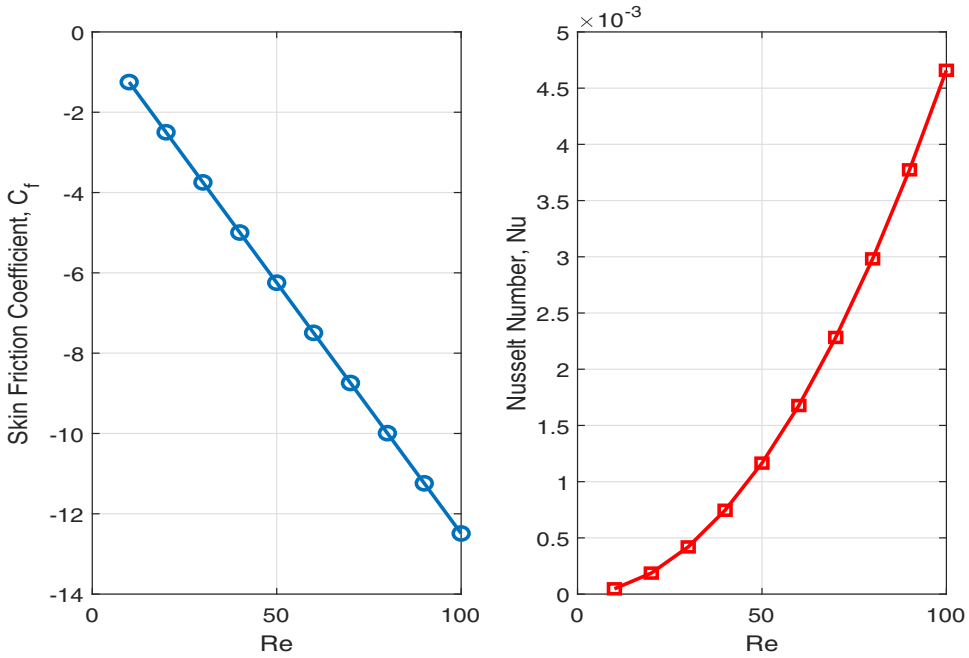

FIGURE 13 | Variation of Re on C_f and Nu. [Color figure can be viewed at wileyonlinelibrary.com]

Additionally, the analysis reveals that the local skin friction coefficient reduces with decreasing values of both the Prandtl number (Pr) and the viscosity parameter (β_1). These results are in close conformity with the earlier study of Nasrin and Alim [18].

6 | Conclusion

This study has presented a comprehensive analysis of the thermodynamic irreversibility in steady viscous Couette flow with convective cooling and temperature-dependent viscosity. The main findings can be summarized as follows:

- Increasing the pressure gradient parameter enhances both velocity and temperature fields, while reducing entropy generation. A 19.60% rise in the pressure gradient parameter decreased the total entropy generation rate by approximately 11.34%, thereby improving thermodynamic efficiency.
- Higher Reynolds numbers intensify momentum and thermal boundary layers, leading to nonmonotonic entropy generation patterns. At $Re = 20$, entropy generation increased by about 8% compared to $Re = 1$, highlighting the competition between viscous and thermal effects.
- Viscosity growth improves thermal retention but lowers velocity and entropy generation; a twofold increase in viscosity reduced entropy generation by nearly 9.08%.
- Larger Eckert numbers (Ec) significantly elevate fluid temperature, yet slightly reduce entropy generation. Raising Ec from 3.50 to 5.0 increased the temperature by 15% while decreasing entropy generation by 12% due to dominant viscous dissipation.
- An increase in Prandtl number (Pr) improves heat transfer efficiency and lowers entropy generation. At $Pr = 5.0$, entropy generation was 6.45% lower than at $Pr = 3.0$.
- Growth in Brinkman number (Br) augments entropy generation through viscous dissipation and shifts irreversibility toward fluid frictional effects.
- Larger Biot numbers (Bi) enhance convective heat transfer, but also intensify entropy generation near the upper wall. Specifically, a 16.39% rise in Bi increased wall entropy production by 9% due to higher thermal gradients.
- Variations in governing parameters significantly influence both the skin friction coefficient (C_f) and Nusselt number (Nu), which are key indicators of irreversibility. While increases in β_1 and Bi reduce Nu with little change in C_f, higher Ec and Re increase Nu by up to 9.63% while reducing C_f by about 3.70%, implying stronger convective heat transfer with diminished frictional resistance.

In conclusion, this study demonstrates that thermodynamic irreversibility in steady viscous Couette flow is highly sensitive to variations in flow and thermal parameters, with both C_f and Nu serving as crucial indicators of entropy generation. Future extensions should focus on transient and three-dimensional models for greater realism, experimental validation of the numerical predictions, and the incorporation of advanced enhancement strategies such as nanofluids, surface texturing, or magnetic field control to further minimize entropy production. Sensitivity and uncertainty analyses are also recommended to ensure reliable performance of Couette flow systems under practical engineering conditions.

7 | Design Recommendations

The present analysis suggests that both geometric and flow-controlling variables play critical roles in minimizing entropy generation and enhancing heat transfer in steady viscous Couette flow. From a geometric perspective, moderate channel spacing should be maintained to avoid excessive shear stresses,

while a sufficiently large aspect ratio ensures fully developed profiles without imposing high pressure losses. The Navier slip parameter emerges as an important design factor: increasing slip at the moving wall reduces wall shear stress and frictional irreversibility, making smooth or surface-treated walls preferable. Similarly, moderate Biot numbers provide a balance between effective convective cooling and manageable thermal gradients, while excessive values, although improving heat transfer, significantly increase local entropy generation near the cooled wall. With respect to flow variables, a positive pressure gradient is beneficial because it simultaneously raises velocity and temperature while lowering total entropy generation, thus improving thermodynamic efficiency more effectively than excessive wall speeds. Moderate Reynolds numbers are recommended for practical designs, since very high values intensify both velocity and thermal boundary layers, leading to complex entropy generation patterns. Lower Eckert and Brinkman numbers should be targeted to minimize viscous heating, although moderate values can still be tolerated when higher heat transfer rates are required. Fluids with higher Prandtl numbers are advantageous because they suppress entropy generation by improving heat transfer efficiency. Overall, the results highlight that optimal design requires careful tuning of A, Re, Ec, Pr, Br, Bi, and β_1 to achieve a compromise between low irreversibility and sufficient convective performance, with C_f and Nu serving as reliable indicators for design evaluation.

Nomenclature

Variable/parameter name	Description (SI unit)
A	pressure gradient parameter $= \frac{\partial P}{\partial x}$
b	distance between plates (m)
$Be(\eta)$	local Bejan number
Bi	Biot number $= \frac{hb}{k}$
Br	Brinkman number $= \frac{\mu_0 U^2}{kT_a}$
C_f	skin-friction coefficient
c_p	specific heat at constant pressure (J/[kg K])
Ec	Eckert number $= \frac{U^2}{C_p T_a}$
h	heat transfer coefficient (W/^{2}K)
k	thermal conductivity (W/[m K])
N_s	dimensionless entropy generation number
$N_{s,t}$	entropy production due to the transfer of heat
$N_{s,v}$	entropy production due to viscous
Nu	Nusselt number
P	pressure (Pa)
Pr	Prandtl number $= \frac{\nu_0}{\alpha}$
Re	Reynolds number $= \frac{Ub}{\nu_0}$
S''_{gen}	local dimensional entropy generation rate (W/[m^3 K])
T	local temperature (K)
T_a	ambient/reference temperature (K)
u	dimensional velocity in the x-direction (m/s)
U	velocity of the top plate (m/s)
W	dimensionless velocity $= u/U$
x, y	spatial coordinates (m)

Greek Symbols

α	thermal diffusivity (m^2/s)
β	temperature–viscosity coefficient (1/K)
β_1	viscosity parameter $= \beta T_a$
ϵ	regularization parameter
η	dimensionless coordinate $= y/b$
μ_0	reference dynamic viscosity (Pa·s)
$\mu(T)$	dynamic viscosity (Pa·s)
ν_0	reference kinematic viscosity (m^2/s)
$\nu(T)$	kinematic viscosity (m^2/s)
ρ	density of fluid (kg/m^3)
θ	dimensionless temperature $= (T - T_a)/T_a$

Author Contributions

All authors were involved throughout the development of the article and have confirmed the final manuscript for submission.

Acknowledgments

The authors extend their appreciation to Dr. Muhammad Faisal (University of Azad Jammu and Kashmir-Pakistan) and Dr. Chacha S. Chacha (University of Dar es Salaam-Tanzania) for their support in MATLAB coding.

Conflicts of Interest

The authors declare no conflicts of interest.

Data Availability Statement

The data sets/code generated and analyzed during this study are available from the corresponding author upon reasonable request.

References

1. K. R. Rajagopal, G. Saccomandi, and L. Vergori, "Couette Flow With Frictional Heating in a Fluid With Temperature and Pressure Dependent Viscosity," *International Journal of Heat and Mass Transfer* 54, no. 4 (2011): 783–789.

2. M. S. Tshehla, O. D. Makinde, and G. E. Okecha, "Heat Transfer and Entropy Generation in a Pipe Flow With Temperature Dependent Viscosity and Convective Cooling," *Scientific Research and Essays* 5, no. 23 (2010): 3730–3741.

3. O. D. Makinde and R. L. Maserumule, "Thermal Criticality and Entropy Analysis for a Variable Viscosity Couette Flow," *Physica Scripta* 78, no. 1 (2008): 015402.

4. O. D. Makinde and A. Aziz, "Second Law Analysis for a Variable Viscosity Plane Poiseuille Flow With Asymmetric Convective Cooling," *Computers & Mathematics With Applications* 60, no. 11 (2010): 3012–3019.

5. M. S. Tshehla and O. D. Makinde, "Analysis of Entropy Generation in a Variable Viscosity Fluid Flow Between Two Concentric Pipes With a Convective Cooling at the Surface," *International Journal of Physical Sciences* 6, no. 25 (2011): 6053–6060.

6. O. D. Makinde and A. S. Eegunjobi, "Entropy Analysis of a Variable Viscosity MHD Couette Flow Between Two Concentric Pipes With Convective Cooling," *Engineering Transactions* 68 (2020): 317–334.

7. M. H. Mkwizu and O. D. Makinde, "Entropy Generation in a Variable Viscosity Channel Flow of Nanofluids With Convective Cooling," *Comptes Rendus Mécanique* 343, no. 1 (2015): 38–56.

8. O. Kigodi, M. H. Mkwizu, A. X. Matofali, et al., "Numerical Investigation of Entropy Generation in Unsteady MHD Generalized Couette Flow With Convective Cooling," *Communication in Mathematical Modeling and Applications* 4, no. 3 (2019): 95–111.

9. E. J. Ndelwa, M. H. Mkwizu, A. X. Matofali, and A. O. Ali, "Entropy Analysis of MHD Hybrid Nanofluid in a Rotating Channel Filled With Porous Material," *International Journal of Thermofluids* 24 (2024): 100887.

10. P. Mondal and D. K. Maiti, "Base Fluids, Its Temperature and Heat Source on MHD Couette–Poiseuille Nanofluid Flow Through Slippy Porous Microchannel With Convective-Radiative Condition: Entropy Analysis," *Journal of Engineering Thermophysics* 32, no. 4 (2023): 835–857.

11. M. Faisal, I. Ahmad, and T. Javed, "Numerical Assessments of Prescribed Heat Sources on Unsteady 3D Flow of Williamson Nanoliquid Through Porous Media," *Special Topics & Reviews in Porous Media: An International Journal* 12, no. 3 (2021): 241–256.

12. M. Sukumar and S. V. K. Varma, "Entropy Generation and Temperature Dependent Heat Source Effects on MHD Couette Flow With Permeable Base in the Presence of Radiation and Viscous Dissipation," *Middle East Journal of Scientific Research* 24, no. 8 (2016): 2577–2588.

13. M. Ali, M. A. Alim, R. Nasrin, and M. S. Alam, "Study the Effect of Chemical Reaction and Variable Viscosity on Free Convection MHD Radiating Flow Over an Inclined Plate Bounded by Porous Medium," *AIP Conference Proceedings* 1754, no. 1 (2016): 040009.

14. R. Nasrin and M. A. Alim, "Entropy Generation by Nanofluid With Variable Thermal Conductivity and Viscosity in a Flat Plate Solar Collector," *International Journal of Engineering, Science and Technology* 7, no. 2 (2015): 80–93.

15. R. Nasrin, M. A. Alim, and A. J. Chamkha, "Natural Convection Flow Across a Nanofluid Layer With Temperature-Dependent Thermal Conductivity and Viscosity," *International Journal of Energy & Technology* 6, no. 2 (2014): 1–9.

16. R. Nasrin, M. A. Alim, and A. J. Chamkha, "Combined Convection Flow in Triangular Wavy Chamber Filled With Water–CuO Nanofluid: Effect of Viscosity Models," *International Communications in Heat and Mass Transfer* 39, no. 8 (2012): 1226–1236.

17. R. Nasrin, M. A. Alim, and A. J. Chamkha, "Effect of Viscosity Variation on Natural Convection Flow of Water–Alumina Nanofluid in an Annulus With Internal Heat Generation," *Heat Transfer—Asian Research* 41, no. 6 (2012): 536–552.

18. R. Nasrin and M. A. Alim, "MHD Free Convection Flow Along a Vertical Flat Plate With Thermal Conductivity and Viscosity Depending on Temperature," *Journal of Naval Architecture and Marine Engineering* 6, no. 2 (2009): 72–83.

19. A. Sene, S. Ben Sadek, S. C. Hirata, and M. N. Ouarzazi, "Onset of Viscous Dissipation Instability in Plane Couette Flow With Temperature-Dependent Viscosity," *Energies* 16, no. 10 (2023): 4172.

20. Y. Demirel, "Thermodynamic Analysis of Thermomechanical Coupling in Couette Flow," *International Journal of Heat and Mass Transfer* 43, no. 22 (2000): 4205–4212.

21. P. K. Mondal and S. Wonwises, "Assesment of Thermodynamic Irreversibility in a Micro-Scale Viscous Dissipative Circular Couette Flow," *Entropy* 20, no. 1 (2018): 50.

22. O. D. Makinde and A. S. Eegunjobi, "Analysis of Inherent Irreversibility in a Variable Viscosity MHD Generalized Couette Flow With Permeable Walls," *Journal of Thermal Science and Technology* 8, no. 1 (2013): 240–254.

23. T. Chinyoka and O. D. Makinde, "Numerical Investigation of Entropy Generation in Unsteady MHD Generalized Couette Flow With Variable Electrical Conductivity," *Scientific World Journal* 2013, no. 1 (2013): 364695.

24. P. Venkatesh, B. J. Gireesha, and F. Almeida, "Investigation of Irreversibilities in a Microchannel by Differing Viscosity, Including Buoyancy Forces and Suction/Injection," *Heat Transfer* 50, no. 4 (2021): 3620–3640.

25. P. Vyas and S. Soni, "Entropy Analysis for MHD Casson Fluid Flow in a Channel Subjected to Weakly Temperature Dependent Convection Coefficient and Hydrodynamic Slip," *Journal of Rajasthan Academy of Physical Sciences* 15, no. 1–2 (2016): 1–18.

26. A. R. Hassan, O. W. Lawal, and F. F. Amurawaye, "Thermodynamic Analysis of a Variable Viscosity Reactive Hydromagnetic Couette Flow Within Parallel Plates," *Tanzania Journal of Science* 47, no. 2 (2021): 432–441.

27. P. Vyas and S. Khan, "Dual Entropy Regime in Channel Flow Subjected to Temperature Dependent Convection Mechanism," *International Journal of Heat & Technology* 39, no. 2 (2021): 424–432.

28. M. Faisal, F. Mabood, I. A. Badruddin, M. Aiyaz, and F. M. Butt, "Entropic Behavior With Activation Energy in the Dynamics of Hyperbolic–Tangent Mixed-Convective Nanomaterial Due to a Vertical Slendering Surface," *Multidiscipline Modeling in Materials and Structures* 20, no. 2 (2024): 341–362.

29. A. O. Ajibade and T. U. Onoja, "Entropy Generation Due to Natural Convection Couette Flow of Viscous Incompressible Fluids in a Vertical Parallel Porous Channel," *Journal of the Nigerian Mathematical Society* 40, no. 3 (2021): 183–204.

30. F. A. Zahor, R. Jain, A. O. Ali, and V. G. Masanja, "Modeling Entropy Generation of Magnetohydrodynamics Flow of Nanofluid in a Porous Medium: A Review," *International Journal of Numerical Methods for Heat & Fluid Flow* 33, no. 2 (2023): 751–771.

31. M. H. Mkwizu, A. X. Matofali, and N. Ainea, "Entropy Generation in a Variable Viscosity Transient Generalized Couette Flow of Nanofluids With Navier Slip and Convective Cooling," *International Journal of Advances in Applied Mathematics and Mechanics* 5, no. 4 (2018): 20–29.

32. N. U. B. Varma, J. L. Ramaprasad, and K. S. Balamurugan, "Impact of Entropy Generation and Temperature Gradient Heat Source on Couette Flow in a Permeable Magnetic Field," *Heat Transfer* 53, no. 5 (2024): 2509–2524.

33. I. S. Mfinanga and A. Iddi, "Effect of Magnetic Field on the Wall Permeable Channel Flow With Convective Cooling," *International Journal of Advances in Scientific Research and Engineering (IJASRE)* 6, no. 5 (2020): 51–65, https://doi.org/10.31695/IJASRE.2020.33802.

34. B. K. Jha and Y. J. Danjuma, "Impact of Variable Viscosity on Unsteady Couette Flow," *Heat Transfer* 54, no. 3 (2025): 2032–2048.

35. M. A. Mjankwi, V. G. Masanja, E. W. Mureithi, and M. N. O. James, "Unsteady MHD Flow of Nanofluid With Variable Properties Over a Stretching Sheet in the Presence of Thermal Radiation and Chemical Reaction," *International Journal of Mathematics and Mathematical Sciences* 2019, no. 1 (2019): 7392459.

36. M. Qasim, Z. Ali, U. Farooq, and D. Lu, "Investigation of Entropy in Two-Dimensional Peristaltic Flow With Temperature Dependent Viscosity, Thermal and Electrical Conductivity," *Entropy* 22, no. 2 (2020): 200, https://doi.org/10.3390/e22020200.

37. M. I. Afridi and M. Qasim, "Second Law Analysis of Blasius Flow With Nonlinear Rosseland Thermal Radiation in the Presence of Viscous Dissipation," *Propulsion and Power Research* 8, no. 3 (2019): 234–242, https://doi.org/10.1016/j.jppr.2018.06.001.

38. Z. Ali, M. Qasim, and M. U. Ashraf, "Thermodynamic Analysis of Nonlinear Convection in Peristaltic Flow," *International Communications in Heat and Mass Transfer* 129 (2021): 105686, https://doi.org/10.1016/j.icheatmasstransfer.2021.105686.

39. K. S. Balamurugan, N. U. B. Varma, and J. L. Ramaprasad, “Entropy Generation Analysis on Forced and Free Convection Flow in a Vertical Porous Channel With Aligned Magnetic Field and Navier Slip,” *Heat Transfer* 52, no. 7 (2023): 4619–4635, https://doi.org/10.1002/htj.22897.

40. K. S. Balamurugan, N. U. B. Varma, and J. L. Ramaprasad, “Heat Transfer and Entropy Generation Analysis in a Horizontal Channel Filled With a Permeable Medium in the Presence of Aligned Magnetic Field and Temperature Gradient Heat Source,” *SN Applied Sciences* 3, no. 1 (2021): 377, https://doi.org/10.1007/s42452-021-04380-3.

41. K. Balamurugan, N. U. B. Varma, and J. Ramaprasad, “Entropy Generation and Temperature Gradient Heat Source Effects on MHD Couette Flow With Permeable Base in the Presence of Viscous and Joule's Dissipation,” *Frontiers in Heat and Mass Transfer* 15, no. 1 (2020): 1–7, https://doi.org/10.5098/hmt.15.8.

42. V. B. Rajakumar Komaravolu, T. G. Rao, K. S. Balamurugan, and C. B. Rani, “Cross-Diffusion Effects on Magnetohydrodynamic Free Convective Flow Over a Vertical Porous Plate Under the Influence of Chemical Reactions, Thermal Radiation, and Dissipative Heating,” *Heat Transfer* 54, no. 5 (2025): 3374–3391, https://doi.org/10.1002/htj.23358.

43. M. Qasim, Z. Hayat Khan, I. Khan, and Q. M. Al-Mdallal, “Analysis of Entropy Generation in Flow of Methanol-Based Nanofluid in a Sinusoidal Wavy Channel,” *Entropy* 19, no. 10 (2017): 490, https://doi.org/10.3390/e19100490.

44. M. I. Afridi, Z. Ali, and M. Qasim, “Entropy Production in the Flow of Bingham–Papanastasiou Fluid Having Temperature and Shear Rate-Dependent Viscosity,” *Numerical Heat Transfer, Part B: Fundamentals* 75, no. 4 (2024): 234–249, https://doi.org/10.1080/10407790.2024.2341093.

45. O. D. Makinde, W. A. Khan, and A. Aziz, “On Inherent Irreversibility in Sakiadis Flow of Nano Fluids,” *International Journal of Exergy* 13, no. 2 (2013): 159–174.

46. A. S. Eegunjobi and O. D. Makinde, “Entropy Generation Analysis in a Variable Viscosity MHD Channel Flow With Permeable Walls and Convective Heating,” *Mathematical Problems in Engineering* 2013, no. 1 (2013): 630798.

47. M. H. Mkwizu, O. D. Makinde, and Y. Nkansah-Gyekye, “Numerical Investigation into Entropy Generation in a Transient Generalized Couette Flow of Nanofluids With Convective Cooling,” *Sadhana* 40 (2015): 2073–2093.

48. M. H. Carpenter, C. A. Kennedy, H. Bijl, S. A. Viken, and V. N. Vatsa, “Fourth-Order Runge–Kutta Schemes for Fluid Mechanics Applications,” *Journal of Scientific Computing* 25 (2005): 157–194.

49. S. J. Chapman, *MATLAB Programming for Engineers* (Brooks/Cole Publishing Co., 2001).